Continuous Calibration of Microring Weights for Analog Optical Networks

Alexander N. Tait, Thomas Ferreira de Lima, Mitchell A. Nahmias, Bhavin J. Shastri, *Member, IEEE*, and Paul R. Prucnal, *Fellow, IEEE*

***Abstract*— Continuously configurable weighted addition is a key function for multivariate analog signal processing. The wavelength-division multiplexed version of weighted addition based on microrings can apply the strengths of photonic integration, wideband photonic information processing, and multi-wavelength networks toward new approaches to ultrafast analog distributed processing. In this letter, we experimentally demonstrate single-channel functionality using a 5-GHz signal, showing a continuous range of complementary (+/−) weighting in a bank of silicon microrings using a feedforward controller and balanced detection technique. Weight tuning accuracy with a dynamic range of 9.2 dB (i.e., 3.1 bits) is shown, and steps to improve performance are discussed. Systems of more microring weights and weight banks could address hitherto unsolvable problems in real-time radio frequency processing and high-performance control.**

***Index Terms*— Photonic integrated circuits, optical signal processing, microwave photonics, neural network hardware, silicon photonics, microresonators.**

I. Introduction

THE RAPID development of CMOS-compatible photonic interconnect technologies has opened a door for unconventional circuit and system opportunities. At the same time, microelectronic fields have renewed investigation of non-von Neumann architectures due, in part, to incipient limitations in aspects of Moore's law [1]. Unconventional processing architectures are often based on the decentralization of processing hardware and co-location of processing and memory. Many unconventional architectures in both microelectronic and photonic substrates take inspiration (or at least terminology) from neuroscience [2]. In the past, neural interconnects implemented in holograms [3] and fiber [4] have failed to outperform mainstream electronics at relevant problems in computing, which can largely be attributed to incompatibility with mainstream integration technologies. Research in semiconductor laser dynamics for neuron-inspired processing has suggested the possibility of photonic neurons that are manufacturable, scalable, and ultrafast [5]–[7]; however, interconnect schemes capable of supporting an integrated analog optical network of laser neurons have not been shown.

A recent proposal for wavelength-division multiplexed (WDM) "broadcast-and-weight" networks [8] could pave the way to large-scale analog processing networks that are realizable with conventional silicon photonic technology [9]–[11]. Broadcast-and-weight networks would rely heavily on a key subcircuit: microring resonator (MRR)-based weighted addition. Weighted addition is a generic type of analog fan-in, which describes how signals from multiple sources are combined. Processing-networking nodes (PNN) interacting with a loop waveguide each broadcast a unique wavelength to the group [12], as in Fig. 1a. Every PNN can then tap a weighted subset of all signals in the network, which are passively summed in a pair of photodetectors (PD). While the laser process at each node can be relatively simple, the overall network has substantial reconfigurability through the tunable weights. MRR banks are a good candidate for tunable weighting in a broadcast-and-weight network because of their ubiquity in PIC platforms, innate WDM compatibility, and ease of tuning via thermal, carrier, or depletion effects [13].

Prior work showed that effective signal polarity (+/−) could be switched using thermal tuning and a balanced PD [14]. In computational neuroscience, negative effective connections (a.k.a. inhibition) play an essential role for stability [15], coding efficiency [16], [17], and compiling techniques [18]. RF photonic circuits based on matched filtering also always require some way to effect negative weights, a problem that has elicited a variety of approaches in fiber [19], [20], which have long included differential detection [21].

Thermal control has been explored extensively in the context of WDM demultiplexers and modulators [22]–[24]. Commonly, the goal of MRR control is to track a particular point in the resonance relative to the signal carrier wavelength, such as its center or maximum slope point. Feedback control approaches are well-suited to MRR demultiplexer and modulator control, but this is not the case for MRR weight control. A MRR weight must be biased at arbitrary points in the filter roll-off region in order to multiply an optical signal by a continuous range of weight values. WDM signals are never demultiplexed before detection, making it difficult to monitor the complete filter state. While in-ring power monitoring devices could make the filter state easier to monitor [25], even these approaches rely on having a reference signal with consistent average power. In analog networks, signal activity can depend strongly on the weight values, so these signals can not be used as references to estimate weight values.

Manuscript received October 1, 2015; revised November 24, 2015; accepted November 30, 2015. Date of publication January 8, 2016; date of current version March 10, 2016. This work was supported in part by the National Science Foundation (NSF) through the Division of Electrical, Communications and Cyber Systems under Grant 1247298 and in part by the NSF Graduate Research Fellowship Program through the Division of Graduate Education under Grant 1148900. Fabrication support was provided via the Natural Sciences and Engineering Research Council of Canada (NSERC) Silicon Electronic-Photonic Integrated Circuits (SiEPIC) Program. The devices were fabricated by Richard Bojko at the University of Washington Washington Nanofabrication Facility, part of the National Science Foundation's National Nanotechnology Infrastructure Network (NNIN).

The authors are with the Lightwave Communications Laboratory, Department of Electrical Engineering, Princeton University, Princeton, NJ 08544 USA (e-mail: atait@princeton.edu; tlima@princeton.edu; mnahmias@princeton.edu; shastri@ieee.org; prucnal@princeton.edu).

Color versions of one or more of the figures in this letter are available online at http://ieeexplore.ieee.org.

Digital Object Identifier 10.1109/LPT.2016.2516440

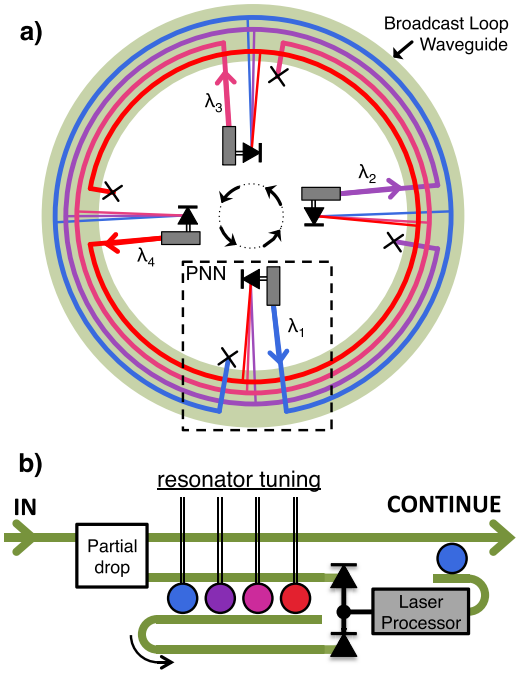

Fig. 1. a) Concept of a broadcast-and-weight network, from [8]. WDM signals are transported between processing-networking nodes (PNNs) by a loop waveguide. b) A PNN circuit [12]. Signals on the bus are partially dropped, then a tunable filter bank independently routes channel power between opposing ports of a balanced photodetector. Continuous weight bank tuning and balanced detection enable effective weights from -1 to $+1$ with one tuning probe per filter. The photodetectors (PD) can act simultaneously as transducers and additive computational elements, solving both challenges of physical fan-in and efficient λ-conversion.

For these reasons, robust weight control must be feedforward and requires offline calibration using known reference signals.

In this work, we demonstrate stable, feedforward control of a single MRR weight over the continuous range from -1 to $+1$. We also examine the repeatability and sources of non-idealities of this approach. Configurable weighted addition is an essential subcircuit for constructing modular, integrated, and analog optical processing networks based on a broadcast-and-weight architecture [8].

II. Methods

Silicon-on-insulator samples are fabricated through UBC SiEPIC [27]; silicon thickness is 220nm with fully etched 500nm wide waveguides. Ti/Au heating contacts are then deposited on top of an oxide passivation layer. The chip is coupled to fiber using focusing subwavelength grating couplers [27]. The weight bank device consists of two bus waveguides and four 6-8μm radius MRRs in a parallel add/drop configuration, each with a thermal tuning element (Fig. 2) that can shift the resonant wavelength via the thermooptic effect. Eigen-mode expansion simulations of the 500 $\times$ 220nm strip waveguide indicate a TE group index of 4.2, which agrees with measured free-spectral range (FSR) of a 6μm radius MRR, which was 15nm. Gaps between bus and ring waveguides are 200nm targeting, a power coupling coefficient of 4%, resulting in measured loaded Q's in the range of 10,000 – 25,000 (Fig. 3). Peak splitting as much as 0.07nm (9GHz) indicates that backscatter coupling had a significant impact on Q and excess loss in this sample [26]. The sample is mounted on a temperature-controlled

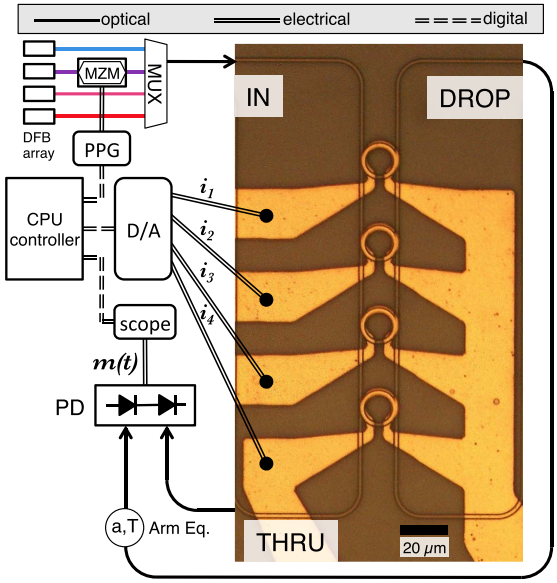

Fig. 2. Experimental setup, including optical micrograph of the fabricated 4-filter weight bank, wherein all filters drop into the same waveguide. Tuning currents i_n are applied to heat each MRR filter (common sink connection not shown). The input consists of a 5Gbps PRBS signal, modulated on an optical carrier at $\lambda_c = 1548.65$nm. The DROP and THRU outputs of the filter bank, after fixed arm amplitude and delay (a, T) equalization, are sent to opposing ports of a balanced PD, yielding the weighted signal, $m(t)$. A CPU controller, interfaced with a pulse pattern generator (PPG), D/A converter and current driver, and oscilloscope (scope), estimates the effective weight value and performs automated weight calibration. Not shown: optical spectrum analyzer and tunable laser source.

alignment stage. The experimental setup consists of computer-controlled instruments for generating optical signals, applying current to the sample, and measuring the resultant weighted output. A digital pulse pattern generator (PPG) produces a PRBS signal at 5Gbps (limited by photodetector bandwidth), and is used for convenience and programmability, although signals are treated as analog. A transmission spectrum analyzer (not shown) is also connected to the device to monitor the filter resonance peaks, and tune them onto resonance with the WDM input signals (Fig. 3). Once filters are roughly matched to signals using spectral measurements, continuous weight calibration proceeds in two steps: 1) drive current to resonance detuning and 2) detuning to effective weight.

The mapping from drive current to resonance wavelength detuning is proportional to temperature shift and related to drive current by:

$$\Delta\lambda = K\,\Delta i_d^2 R(i_{d,0}^2 + \Delta i_d^2) \tag{1}$$

where $\Delta\lambda \equiv \lambda - \lambda_0$ is resonance detuning, K is an effective thermo-optic coefficient, $\Delta i_d^2 \equiv i_d^2 - i_{d,0}^2$ is current-squared detuning, and resistive self-heating is described by

$$R(i_d^2) = R_{amb} + \alpha R(i_d^2) i_d^2 = \frac{R_{amb}}{1 - \alpha i_d^2} \tag{2}$$

where α is a coefficient assumed constant within the range of interest. The model experiences nonlinearity due to self-heating and even thermal runaway at $i_d^2 = \frac{1}{\alpha}$; however, we found it was sufficient to approximate heater resistance to first-order around the on-resonance condition, such that $R(i_{d,0}^2 + \Delta i_d^2) \approx R(i_{d,0}^2)$. While this approximation seems minor, it is only possible because further calibration steps compensate

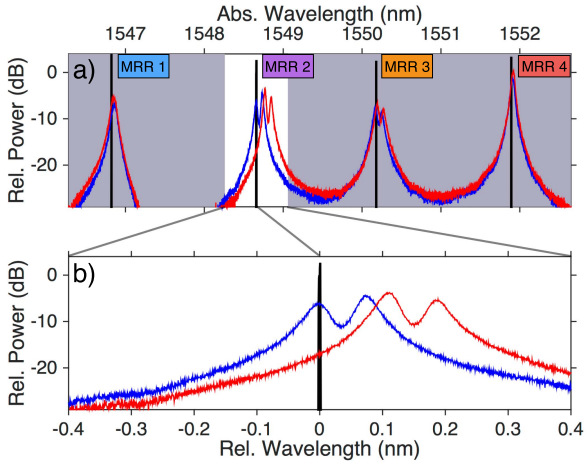

Fig. 3. Spectral measurements of device under test a) Four microring (MRR) filter peaks are independently tuned onto resonance (blue) with a WDM input signal (black). MRR 2 is slightly detuned (red), while other filters are not affected. Channel spacing is 200GHz ± 20GHz (1.6nm ± 0.16nm), and does not need to be consistent because MRRs can be tuned onto resonance over a range of about 14nm. b) Expanded view of the second filter peak, showing a resonance detuning of 0(blue) and 0.1nm(red). The filter transmissivity at the signal wavelength is sensitive over this small range. X-axis is relative to the signal wavelength. The dip in the center of the filter spectrum is unintentional: caused by backscatter coupling between counter-propagating modes [26].

the nonlinear self-heating effects. In devices with multiple channels experiencing thermal cross-talk, a linear thermal model may not be accurate enough to calibrate for cross-talk.

In order to determine the detuning that effects a desired/commanded weight, two calibration sweeps are performed. First, the filter resonance is detuned far from the carrier wavelength, where almost no input power goes to the drop port, and a signal reference, $r(t)$, is measured and stored. The effective weight, μ, of a measured signal, $m(t)$, is here defined as a normalized projection onto this reference:

$$\mu \equiv \frac{\langle r(t) \cdot m(t) \rangle_t}{\langle r(t) \cdot r(t) \rangle_t} = f(\Delta\lambda) \tag{3}$$

where $\langle \cdot \rangle_t$ is a time average. The projection-based approach is used instead of simple RMS in order to reduce the effect of noise when the weight is near zero. Effective weight is an unknown function, f, of detuning. To estimate f, the tuning current is swept so the filter goes through resonance while the effective weight is monitored (Fig. 4a,b). A linear interpolation of the measured points provides an estimate of the weight function. The calibrated control rule is then simply the function inverse:

$$\Delta\lambda \leftarrow \hat{f}^{-1}(\hat{\mu}) \tag{4}$$

where $\hat{f}$ is the estimated tuning function and $\hat{\mu}$ is the command weight. Because of the sharp nonlinearity of f, its initial estimate is poorly sampled, leading to an inaccurate calibration. The calibration is refined by performing a second sweep over $\hat{\mu}$ and updating the estimate of $\hat{f}$ with a more uniformly sampled dataset. Once calibrated, a sweep over command weight is used to assess the accuracy of the controller (Fig. 4c, d). In Fig. 4b, weight values extend below -1 because the DROP/THRU arms were not exactly balanced in amplitude; however, the values outside -1 to $+1$ are simply ignored in this case (Fig. 4d).

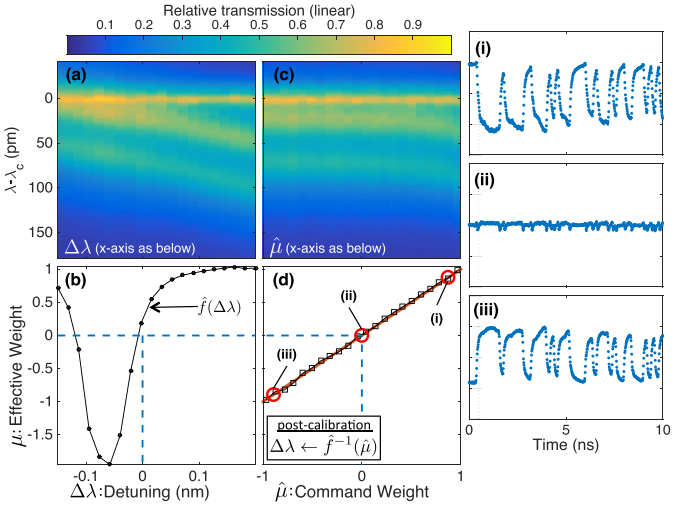

Fig. 4. (a-b) Initial sweep in detuning: (a) shows filter relative transmission spectra vs. resonance detuning (i.e. $\Delta\lambda = \lambda - \lambda_0$). The input optical signal, which is stronger than the spectrum analyzer's swept laser source, is visible at $\lambda - \lambda_c = 0$. (b) Measured weight vs. detuning, showing a full range from -1 to $+1$. Weight values are calculated based on Eq. (3). This curve is used as an estimate of the tuning function $\hat{f}$. (c-d) Calibrated sweep in command weight: (c) the shift in filter resonant wavelength is a strongly nonlinear function of the command weight, which roughly reflects the inverse of the tuning function estimate from (b), such that in (d), there is a well-controlled correspondence between command and measured effective weight. The ideal x = y line is plotted in red. (i-iii) Time traces of the weighted output when the effective weight is positive (i), zero (ii), and negative (iii). Cancellation at zero is not perfect because the 5Gbps signal distorts slightly when crossing the MRR.

III. Results and Discussion

The result of tuning sweep calibration shown in Fig. 4d indicates that simple resonance tuning with feedforward calibration is sufficient to reliably attain a continuous range of analog weight values. Fig. 4(i-iii) show in the time domain that the signal effectivity can be inverted by using the balanced PD and only one tuning degree-of-freedom. The zero-weight output in Fig. 4(ii) is not exactly cancelled. Although the drop and through port power ratios can be balanced, the dispersive effects of of the filter are not accounted for in the present calibration model. This effect might be improved by using coupling modulation, as opposed to resonance tuning, in order to move the signal away from the highly dispersive filter edge [28].

Fig. 5 shows a high-resolution test of the stored calibration model of 5 sweeps over 44 distinct command weights, without intermediate recalibration. This data indicate a dynamic range (i.e. range divided by maximum error) of the weight controller of 9.2dB, in other words, the ability to reliably set the weight with a 3.1 bit precision. From this figure, it is also apparent that the error is dominated by repeatable inaccuracies (±0.096), as opposed to noise standard deviation (±0.053). This means that improvements to the controller accuracy will most likely take the form of more sophisticated calibration methods; for example, iterating more times and/or rejecting outlying data points during function estimation and interpolation. Improvements to the controller algorithm could then yield a noise-limited resolution of 4.2 bits (dynamic range of 12.7dB). Sources of non-repeatable inaccuracy are most likely dominated by polarization drift in the fiber system impacting fiber-to-chip coupling efficiency, and, to a lesser extent, ambient thermal

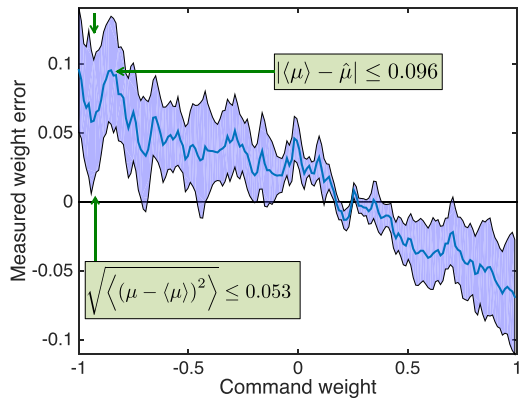

Fig. 5. Repeatability of calibrated weight control versus commanded weight values, $\hat{\mu}$, showing data from 5 sweeps following a single calibration. Errors that are repeatable between trials manifest as offsets to the mean error ($|\langle\mu\rangle - \hat{\mu}|$, solid blue line), whereas errors that are unrepeatable, such as noise, manifest by widening the standard deviation envelope (RMS($\mu - \langle\mu\rangle$), pale blue area). In this experiment, repeatable errors are dominant, which suggests that accuracy can be improved with a more robust calibration algorithm.

fluctuations in the temperature-controlled silicon photonic chip. Polarization control is not an issue for light generated on-chip, and could be ameliorated in fiber experiments by using polarization maintaining fiber or polarization splitting fiber-to-chip couplers.

The interpolation-based calibration approach of measuring points over the entire range is robust to inaccuracy in physical models, as errors will be observed in the weight transfer function f. For multiple channels; however, the number of required measurements using this approach would scale exponentially with channel number because, in general, tuning states affect one another via thermal cross-talk. The challenges for further work controlling multiple channels simultaneously–without exponentially growing calibration time–will include a model-based approach to thermal physics and a procedure for fitting the parameters in Eqs. (1) and (2) based on measurements.

IV. Conclusion

This letter focused on the control of a single MRR weight within a WDM weight bank, showing an initial dynamic range of 9.2dB. Further work will investigate simultaneous tuning of multiple channels, in which inter-MRR thermal and/or optical cross-talk will likely become a source of error. An investigation of how tuning the weight through a sharp MRR filter edge will affect dispersion is also important for understanding bandwidth performance, as well as how bandwidth trades off with channel spacing. Continuous control of a single MRR weight is a key step towards the goal of multivariate analog signal processing in a silicon photonic platform.

Acknowledgment

The authors thank Siamak Abbaslou for helpful discussion on fiber-to-chip alignment.

References

[1] J. Hasler and B. Marr, "Finding a roadmap to achieve large neuromorphic hardware systems," *Frontiers Neurosci.*, vol. 7, no. 118, pp. 1–29, 2013.
[2] G. Indiveri *et al.*, "Neuromorphic silicon neuron circuits," *Frontiers Neurosci.*, vol. 5, no. 73, pp. 1–23, 2011.
[3] P. Asthana, G. P. Nordin, A. R. Tanguay, Jr., and B. K. Jenkins, "Analysis of weighted fan-out/fan-in volume holographic interconnections," *Appl. Opt.*, vol. 32, no. 8, pp. 1441–1469, Mar. 1993.
[4] M. T. Hill, E. E. E. Frietman, H. de Waardt, G.-D. Khoe, and H. J. S. Dorren, "All fiber-optic neural network using coupled SOA based ring lasers," *IEEE Trans. Neural Netw.*, vol. 13, no. 6, pp. 1504–1513, Nov. 2002.
[5] M. A. Nahmias, B. J. Shastri, A. N. Tait, and P. R. Prucnal, "A leaky integrate-and-fire laser neuron for ultrafast cognitive computing," *IEEE J. Sel. Topics Quantum Electron.*, vol. 19, no. 5, Sep./Oct. 2013, Art. ID 1800212.
[6] W. Coomans, L. Gelens, S. Beri, J. Danckaert, and G. Van der Sande, "Solitary and coupled semiconductor ring lasers as optical spiking neurons," *Phys. Rev. E*, vol. 84, no. 3, p. 036209, 2011.
[7] F. Selmi, R. Braive, G. Beaudoin, I. Sagnes, R. Kuszelewicz, and S. Barbay, "Relative refractory period in an excitable semiconductor laser," *Phys. Rev. Lett.*, vol. 112, no. 18, p. 183902, May 2014.
[8] A. N. Tait, M. A. Nahmias, B. J. Shastri, and P. R. Prucnal, "Broadcast and weight: An integrated network for scalable photonic spike processing," *J. Lightw. Technol.*, vol. 32, no. 21, pp. 3427–3439, Nov. 1, 2014.
[9] D. Liang *et al.*, "Hybrid silicon evanescent approach to optical interconnects," *Appl. Phys. A*, vol. 95, no. 4, pp. 1045–1057, 2009.
[10] S. Assefa, F. Xia, and Y. A. Vlasov, "Reinventing germanium avalanche photodetector for nanophotonic on-chip optical interconnects," *Nature Lett.*, vol. 464, pp. 80–84, Mar. 2010.
[11] J. S. Orcutt *et al.*, "Open foundry platform for high-performance electronic-photonic integration," *Opt. Exp.*, vol. 20, no. 11, pp. 12222–12232, May 2012.
[12] M. A. Nahmias, A. N. Tait, B. J. Shastri, T. F. de Lima, and P. R. Prucnal, "Excitable laser processing network node in hybrid silicon: Analysis and simulation," *Opt. Exp.*, vol. 23, no. 20, pp. 26800–26813, Oct. 2015.
[13] P. Dong *et al.*, "Low V_{pp}, ultralow-energy, compact, high-speed silicon electro-optic modulator," *Opt. Exp.*, vol. 17, no. 25, pp. 22484–22490, 2009.
[14] A. Tait *et al.*, "Balanced WDM weight banks for analog optical processing and networking in silicon", in *Proc. IEEE/OSA Summer Topicals*, pp. 21–22, no. MC2.3, Jul. 2015.
[15] A. R. Aron, "The neural basis of inhibition in cognitive control," *Neuroscientist*, vol. 13, no. 3, pp. 214–228, 2007.
[16] P. D. King, J. Zylberberg, and M. R. DeWeese, "Inhibitory interneurons decorrelate excitatory cells to drive sparse code formation in a spiking model of V1," *J. Neurosci.*, vol. 33, no. 13, pp. 5475–5485, 2013.
[17] H. J. Alitto and Y. Dan, "Function of inhibition in visual cortical processing," *Current Opinion Neurobiol.*, vol. 20, no. 3, pp. 340–346, 2010.
[18] T. C. Stewart and C. Eliasmith, "Large-scale synthesis of functional spiking neural circuits," *Proc. IEEE*, vol. 102, no. 5, pp. 881–898, May 2014.
[19] M. P. Chang, A. Tait, J. Chang, and P. R. Prucnal, "An integrated optical interference cancellation system," in *Proc. 23rd Wireless Opt. Commun. Conf. (WOCC)*, May 2014, pp. 1–5.
[20] A. N. Tait, J. Chang, B. J. Shastri, M. A. Nahmias, and P. R. Prucnal, "Demonstration of WDM weighted addition for principal component analysis," *Opt. Exp.*, vol. 23, no. 10, pp. 12758–12765, May 2015.
[21] S. Sales, J. Capmany, J. Marti, and D. Pastor, "Experimental demonstration of fiber-optic delay line filters with negative coefficients," *Electron. Lett.*, vol. 31, no. 13, pp. 1095–1096, Jun. 1995.
[22] R. Amatya, C. W. Holzwarth, H. I. Smith, and R. J. Ram, "Precision tunable silicon compatible microring filters," *IEEE Photon. Technol. Lett.*, vol. 20, no. 20, pp. 1739–1741, Oct. 15, 2008.
[23] C. Qiu, J. Shu, Z. Li, X. Zhang, and Q. Xu, "Wavelength tracking with thermally controlled silicon resonators," *Opt. Exp.*, vol. 19, no. 6, pp. 5143–5148, Mar. 2011.
[24] J. C. C. Mak, W. D. Sacher, T. Xue, J. C. Mikkelsen, Z. Yong, and J. K. S. Poon. (Jul. 2015). "Automatic resonance alignment of high-order microring filters." [Online]. Available: http://arxiv.org/abs/1507.02129
[25] S. Grillanda *et al.*, "Non-invasive monitoring and control in silicon photonics using CMOS integrated electronics," *Optica*, vol. 1, no. 3, pp. 129–136, Sep. 2014.
[26] G. C. Ballesteros, J. Matres, J. Martí, and C. J. Oton, "Characterizing and modeling backscattering in silicon microring resonators," *Opt. Exp.*, vol. 19, no. 25, pp. 24980–24985, Dec. 2011.
[27] Y. Wang *et al.*, "Focusing sub-wavelength grating couplers with low back reflections for rapid prototyping of silicon photonic circuits," *Opt. Exp.*, vol. 22, no. 17, pp. 20652–20662, 2014.
[28] W. D. Sacher *et al.*, "Coupling modulation of microrings at rates beyond the linewidth limit," *Opt. Exp.*, vol. 21, no. 8, pp. 9722–9733, Apr. 2013.